Role of Metal Ions in Catalysis by Enolase: An Ordered Kinetic Mechanism for a Single Substrate Enzyme†

Russell R. Poyner, W. W. Cleland, and George H. Reed*

Department of Biochemistry, University of Wisconsin−Madison, Madison, Wisconsin 53705

Received February 26, 2001; Revised Manuscript Received May 14, 2001

ABSTRACT: Spectroscopic and kinetic methods have been used to explore the roles of divalent metal ions in the enolase-catalyzed dehydration of 2-phosphoglycerate (2-PGA). Enolase requires 2 equiv of metal ion per active site for maximal activity. Previous crystallographic studies [Larsen, T. M., Wedekind, J. E., Rayment, I., and Reed, G. H. (1996) *Biochemistry 35*, 4349−4358] showed that both magnesium ions coordinated to the carboxylate group of the substrate/product—a scheme consistent with metal ion assistance in formation of the enolate intermediate. Electron paramagnetic resonance (EPR) data with ^{17}O-labeled forms of phosphoenolpyruvate show that Mn^{2+}, bound at the lower affinity site, coordinates to one carboxylate oxygen and one phosphate oxygen of the substrate. These observations are fully consistent with the crystallographic data. Plots of activity versus log [metal ion] are bell-shaped, and the inhibitory phases of the profiles have been previously attributed to binding of metal ions at ancillary sites on the enzyme. However, the activation profiles and measurements of ^2H kinetic isotope effects support an ordered kinetic mechanism wherein binding of 2-PGA precedes binding of the second metal ion, and release of the second metal ion occurs prior to departure of phosphoenolpyruvate. High concentrations of metal ion lead to inhibition in the ordered mechanism by interfering with product release. The ^2H kinetic isotope effect is diminished in the inhibitory phases of the metal ion activation profiles in a manner that is consistent with the predominantly ordered mechanism. Zn^{2+} gives lower maximal activity than Mg^{2+}, apparently due to slow release of Zn^{2+} from the product complex. Addition of imidazole increases the maximal rate apparently by accelerating the release of Zn^{2+} from the enzyme.

Enolase (EC 4.2.1.11) catalyzes a β-elimination reaction that removes the elements of water from 2-PGA[1] to form P-enolpyruvate. Evidence from isotope exchange experiments (*2*), kinetic isotope effects (*3*), and site-directed mutagenesis (*4*) indicates that the reaction occurs in a stepwise manner wherein a base on the enzyme removes the nonacidic proton from C2 of 2-PGA prior to the elimination of OH^- from C3 to form product. Multiple proposals exist for the identity of the base responsible for abstraction of the C2 proton of 2-PGA. An early proposal for the catalytic base was a hydroxide ion situated between the carboxyl groups of Glu 211 and Glu 168 (*5*−*7*). Site-directed mutagenesis studies (*4*) and more recent crystallographic studies (*8*−*10*) have indicated that the base responsible for removing the C2 proton of 2-PGA in the first step of the reaction is the ϵ-amino group of Lys 345. Alternatively, His 159 has been proposed to be the base (*11*−*13*). One high-resolution crystal structure (1.8 Å resolution) of enolase is available with the active site occupied by two metal ions and the equilibrium mixture of 2-PGA and P-enolpyruvate (*9*). The $F_o - F_c$ electron density map from ref *9* unambiguously determines the position of 2-PGA/P-enolpyruvate in the active site (Figure 1A). Although hydrogen atoms do not appear in the electron density map, the C2 proton of 2-PGA can be modeled using bond lengths and angles from the structure of Na_3 2-PGA (*14*). Modeling the hydrogen into the structure places it 2.45 Å (*9*) from the ϵ-nitrogen of Lys 345 but more than 5.2 Å from the nearest nitrogen of His 159 and on the opposite side of the substrate (Figure 1B).

Numerous proposals also exist for the acid that promotes elimination of the OH group from C3 of 2-PGA. These include one of the active site metal ions (*5*, *11*, *15*), the imidazole group of His 373 (*12*), and the carboxyl group of Glu 211 (*4*, *10*). The OH group of 2-PGA lies near three ionizable residues, His 373, Glu 168, and Glu 211 (Figure 1) (*9*, *16*). Mutation of His 373 to Asn yields an enzyme with 10% of wild-type activity (*10*, *17*), which suggests a hydrogen-bonding role for this residue. Mutation of either Glu 211 or Glu 168 to Gln results in substantial loss of activity (*4*, *6*, *7*). Analysis of the reactivity of these mutants

† This research was supported in part by NIH Grants GM35752 (G.H.R.) and GM18938 (W.W.C). A preliminary account of part of this research was published in the Proceedings of the 1998 Steenbock Symposium [Poyner, R. R., and Reed, G. H. (1999) in *Enzymatic Mechanisms* (Frey, P. A., and Northrop, D. B., Eds.) pp 300−307, IOS Press, Amsterdam, The Netherlands].

* Address correspondence to this author: University of Wisconsin−Madison, 1710 University Ave., Madison, WI 53705. E-mail: reed@biochem.wisc.edu.

[1] Abbreviations: 2-PGA, 2-phospho-D-glycerate; P-enolpyruvate, phosphoenolpyruvate; PhAH, phosphonoacetohydroxamate; Hepes, *N*-(2-hydroxyethyl)piperazine-*N*′-2-ethanesulfonic acid; TAPS, *N*-tris-(hydroxymethyl)methyl-3-aminopropanesulfonic acid; CHES, 2-(*N*-cyclohexylamino)ethanesulfonic acid; Tris, tris(hydroxymethyl)aminomethane; BisTris, bis(2-hydroxyethyl)iminotris(hydroxymethyl)methane; TCA, trichloroacetic acid; OAc, acetate; EPR, electron paramagnetic resonance; MALDI-TOF mass spectrometry, matrix-assisted laser desorption ionization time-of-flight mass spectrometry. Kinetic parameters preceded by a superscript D are deuterium (^2H) isotope effects on the respective parameter.

10.1021/bi0103922 CCC: $20.00
Published on Web 06/12/2001

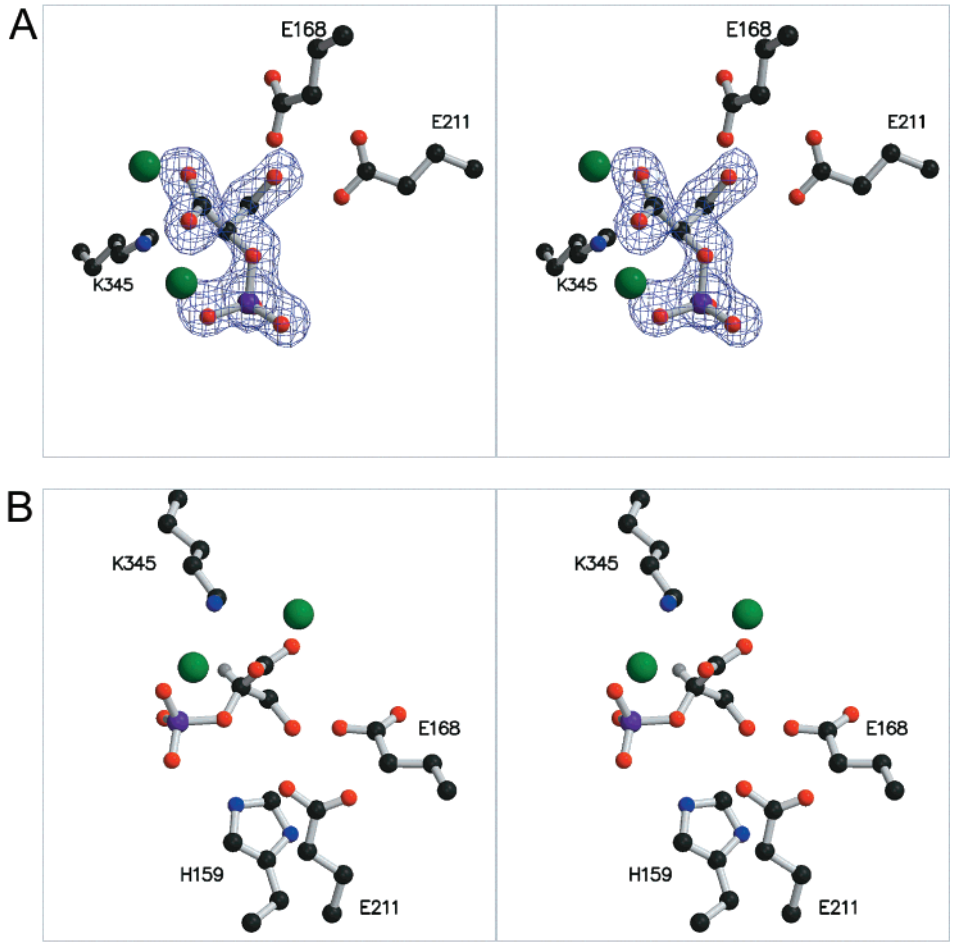

FIGURE 1: Stereoviews of the active site of enolase obtained from the crystal structure of the complex of enolase with the equilibrium mixture of 2-PGA and P-enolpyruvate. (A) Structure including the $F_o - F_c$ electron density for 2-PGA/P-enolpyruvate. (B) Structure showing the predicted position of the C2 proton and its proximity to the ϵ-amino group of Lys 345. Coordinates (PDB file 1ONE) and electron density are from Larsen et al. (*9*). Figures were prepared using Molscript (*56*) and Raster3D (*57*).

with the alternative substrate 3-chloro-P-enolpyruvate indicates that Glu 211 is the acid responsible for promoting the elimination of OH (*4*). The anti stereochemistry of the elimination (*18*) requires the base and acid residues to lie on opposite sides of the substrate. The Lys 345/Glu 211 base/acid pair (*4*) satisfies this criterion, whereas the more recently proposed His 159/His 373 pair (*12*, *13*) does not. Moreover, the H159A mutant enolase is reported to have >1% of wild-type activity when assayed at millimolar concentrations of Mg^{2+} (*58*).

Each active site of enolase requires 2 equiv of Mg^{2+} (*19*) or other divalent cation to achieve maximal activity. The first metal ion binds to the protein with high affinity in the absence of substrate, and a second metal ion binds in the presence of substrate (*19*). The crystal structure of the bis-magnesium complex with an equilibrium mixture of substrate and product (*20*) shows that both magnesium ions are coordinated to the carboxylate group of the substrate/product (Figure 1). This arrangement implicates the metal ions, together with the protonated ϵ-amino group of Lys 396, in stabilization of the enolate intermediate.

For enolase, plots of activity versus log $[M^{2+}]$ exhibit a characteristic bell shape (*19*, *21*). The shapes of these activation curves—especially the inhibitory region—have not been fully explained. One hypothesis (*12*, *22*) is that, at higher concentrations, metal ions bind at inhibitory sites on the enzyme and that such binding switches off catalytic activity. No such sites have appeared in crystal structures (*10*), and evidence for this hypothesis from direct binding studies is ambiguous. For example, Westhead and co-workers (*23*) found significant inhibition under conditions where less than 2 equiv of Co^{2+} was bound. An ordered kinetic mechanism, in which the second metal ion binds after the substrate and dissociates before the product (Scheme 1), provides another explanation for the bell-shaped activation profiles (*24*, *25*). Faller et al. (*19*) proposed an ordered addition of the substrate and the second metal ion. Extending the order to include the release of the second metal ion and release of product accounts for the shape of the activation curves without a need to postulate additional binding sites for metal ions. The arrangement of the metal ions and the substrate observed in the crystal structure is consistent with an ordered mechanism. The second metal ion binds to one phosphate and one carboxylate oxygen of the substrate and to the carbonyl and hydroxyl oxygens of Ser 39. Ser 39 is

Scheme 1

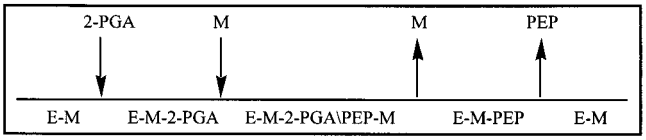

part of a flexible loop that moves to close off the active site upon binding of the second metal (*8*).

There are, however, reports that the second metal ion binds to a site remote from the substrate and activates indirectly (*26*). Experiments reported in the present paper provide independent support for direct binding of the second equivalent of metal ion to the substrate/product in a manner fully consistent with the crystallographic structure. The ordered kinetic mechanism is tested with primary ^{2}H kinetic isotope effects.

EXPERIMENTAL PROCEDURES

Enolase was prepared from active dry yeast using published procedures (*8*). Contaminating metal ions were removed from solutions of enzyme, Hepes buffer, and substrates by passage over a 1 × 20 cm column of Chelex-100 in the K^+ form. Imidazole was purified by recrystallization, first from water as the hydrochloride and then from benzene as the free base. Stock solutions of the purified imidazole were adjusted to pH 7.5 with HCl. High purity (>99.99%) metal chlorides were from Aldrich. Carbamate kinase and carbonic anhydrase were from Sigma. Pyruvate kinase was a gift from Dr. Todd Larsen. Triethylamonium bicarbonate buffer was prepared by bubbling CO_2 into a solution of freshly distilled triethylamine.

Synthesis of 2-Nitroethylphosphonate and 3-Hydroxy-2-nitro-1-phosphonopropane. 2-Nitroethylphosphonate was prepared by a modification of the published procedure (*27*). Diethyl 2-bromoethylphosphonate was converted to diethyl 2-iodoethylphosphonate by reaction with 1 equiv of anhydrous NaI in acetone. The NaBr produced was removed by filtration, and the acetone was evaporated under a stream of dry N_2. The iodo derivative was then dissolved in ether and stirred with 1 equiv of $AgNO_2$ at 4 °C in the dark for 48 h. The reaction was then continued for 24 h at 25 °C. Silver salts were removed by filtration, and the ether was evaporated under a stream of N_2. The ethyl groups were then removed by reaction with bromotrimethylsilane (*28*), and 2-nitroethylphosphonate was purified by anion-exchange chromatography as described previously (*27*). The infrared spectrum of 2-nitroethylphosphonate obtained from a sample in a KBr pellet exhibited a strong absorbance at 1554 cm^{-1} as expected for an alkyl nitro group. The ^{1}H NMR spectrum contained multiplets at 2.3 and 4.8 ppm as described (*27*).

3-Hydroxy-2-nitro-1-phosphonopropane was synthesized by condensing 2-nitroethylphosphonate with formaldehyde and purified by anion exchange as described by Anderson et al. (*27*).

Preparation of [2-^{2}H]-2-PGA. [2-^{2}H]-2-PGA was prepared by exchange of 2-PGA in ^2H_2O using the E211Q variant of enolase. This variant catalyzes the exchange of the proton at C2 of 2-PGA but not the dehydration of 2-PGA (*4*). The exchange was monitored by ^{1}H NMR. When the reaction was complete, enzyme was removed by ultrafiltration, and the product was passed over a column of Chelex-100 to remove metal ions.

Preparation of ^{17}O-Labeled P-enolpyruvate. P-enolpyruvate labeled with ^{17}O in the peripheral phosphate oxygens and the carboxylate oxygens was prepared by a modification of the published procedure (*29*). P-enolpyruvate (8 mg, K^+ salt), 6 mg of KCl, 50 mg of dry Dowex 50W-X8 H^+ form, and 50 μL of $H_2{}^{17}O$ (51.1% ^{17}O) were combined in a 0.5 mL tube. The tube was sealed and heated in a 98 °C water bath for 10 min. The tube was transferred to an ice bath and 250 μL of 1 M Tris base added. Enzymatic assays revealed the solution to be 12 mM in P-enolpyruvate and 72 mM in pyruvate. On the basis of the tabulated rate constants (*29*) the exchange should be ~95% complete under these conditions, leading to P-enolpyruvate 46% enriched in ^{17}O in the oxygens of the carboxylate and nonbridging phosphate groups. Label incorporation was confirmed by MALDI-TOF mass spectrometry of the ammonium salt of P-enolpyruvate. A sample containing ^{16}O was treated in identical fashion. Both samples were purified by anion-exchange chromatography on a 1.5 × 25 cm column of Bio-Rad AG-MP-1, 200−400 mesh, HCO_3^- form. The column was eluted at 2 mL min^{-1} with a 0.5 L linear gradient from 0.25 to 0.5 M triethylamonium bicarbonate, pH 7.5. Fractions containing P-enolpyruvate were pooled and dried by rotary evaporation. Residual triethylamine was removed by two cycles of methanol addition and rotary evaporation.

P-enolpyruvate labeled in the carboxylate oxygens was prepared enzymatically. Pyruvic acid was labeled by incubating 2.8 μL (40 μmol) of freshly distilled pyruvic acid with 20 μL of 51.1% enriched $H_2{}^{17}O$ for 6 days. Under these conditions the exchange of the pyruvate oxygens with water should be >95% complete (*30*) so that pyruvate is expected to be >44% enriched in ^{17}O. Pyruvate was phosphorylated using the couple of pyruvate kinase and carbamate kinase using an excess of carbamyl phosphate. A solution (20 mL) containing 0.1 M carbamyl phosphate, 5 mM ATP, 0.25 mg/mL carbonic anhydrase, 75 mM CHES, 75 mM KCl, 7.5 mM $MgSO_4$, 250 IU mL^{-1} pyruvate kinase, and 5 IU mL^{-1} carbamate kinase was prepared in water freed of CO_2 by boiling. The pH was adjusted to 9.2 with freshly prepared 1 N KOH. Reaction was initiated by addition of 50 μL (20 μmol) of ^{17}O-labeled pyruvate. The reaction mixture was protected from atmospheric CO_2 by a stream of N_2. After 1 h, the reaction was quenched with 10 mL of 2 M TCA. The protein precipitate was removed by centrifugation, and the supernatant was extracted three times with 5 mL portions of ether to remove TCA. The mixture was then adjusted to pH 9 with 1 N KOH.

Several chromatographic steps were required to purify the labeled P-enolpyruvate. The reaction mixture was subjected to two rounds of anion-exchange purification as described above for uniformly ^{17}O-labeled P-enolpyruvate. The sample was then applied to a 1.5 × 25 cm column of Bio-Rad AG-MP-1 resin in the Cl^- form and eluted at 2 mL/min with a 0.9 L linear gradient from 50 to 150 mM LiCl in 10 mM BisTris, pH 6.0. Fractions containing P-enolpyruvate were neutralized with 1 M imidazole, dried by rotary evaporation, and washed with 33% methanol in acetone to remove LiCl. The material was then dissolved in 48 mM KH_2PO_4, 9 mM tetrabutylammonium phosphate, and 10% acetonitrile and passed over a 2.5 × 45 cm column of reverse-phase silica (Merck, Lichroprep RP-18, 20−40 μm) equilibrated with the same buffer. Fractions containing P-enolpyruvate were pooled, and phosphate was removed by anion-exchange chromatography at pH 7.5 as described above. A sample of unlabeled P-enolpyruvate was made from pyruvic acid and purified by the same procedure. A small column of SP-Sephadex S-25 in the K^+ form was used to convert solutions

of P-enolpyruvate to the K^+ form.

Standardization of Stock Solutions. Concentrations of stock solutions of 2-PGA and of P-enolpyruvate were determined by enzymatic end point assays using lactate dehydrogenase and pyruvate kinase for P-enolpyruvate and lactate dehydrogenase, pyruvate kinase, and enolase for 2-PGA. Concentrations of enolase were determined spectrophotometrically ($\epsilon_{280nm} = 0.89$ mL mg^{-1} cm^{-1}) (*31*) using a subunit molecular weight for the subunit of 46 500 (*32*, *33*). Concentrations of various species of Zn^{2+}−imidazole were calculated using stability constants from ref *34*.

Kinetic Measurements. Wild-type enolase was assayed by monitoring the absorbance at 240 nm due to P-enolpyruvate assuming an extinction coefficient of 1.4 mM^{-1} cm^{-1} (*35*). Assay reactions were initiated by addition of ~0.02 μM enolase to solutions containing substrates and metal ions as indicated in the figure legends. Kinetic data with Zn^{2+} in the presence of imidazole were fitted to the equation for linear substrate inhibition (eq 1) (*24*). Otherwise, kinetic data were fitted to the equation for hyperbolic substrate inhibition (eq 2) (*25*).

$$v = \frac{Mk_{cat}E_t}{K_m + M + M^2/K_i} \quad (1)$$

$$v = \frac{Mk_{cat}E_t}{K_m + M\dfrac{1 + M/K_{in}}{1 + M/K_{id}}} \quad (2)$$

In eq 2 K_{in} corresponds to the concentration of metal ion at half-maximal inhibition analogous to K_i in eq 1, and the ratio of K_{in} to K_{id} gives the ratio of k_{cat} to the turnover rate at maximal inhibtion.

The ordered mechanism of Scheme 1 can be simplified by combining the step for interconversion of EM(2-PGA)M and EM(PEP)M with the step for release of the second metal ion and assuming saturating substrate such that free enzyme is negligible. In the simplified Scheme 2, k_3 is a composite rate constant (*36*, *37*) for dehydration of 2-PGA and release of the second metal ion, k_4 is a composite rate constant for binding of the second metal ion in the reverse reaction and hydration of PEP, and k_5 is a composite rate constant for release of PEP and binding of 2-PGA. Equation 1 is easily derived from Scheme 2 by standard methods. This leads to expressions for k_{cat}, K_m, and K_i in terms of the rate constants of Scheme 2 (eqs 3−5).

$$k_{cat} = \frac{k_1k_3k_5}{k_2k_4 + k_1k_5 + k_1k_3} \quad (3)$$

$$K_m = \frac{k_5(k_2 + k_3)}{k_2k_4 + k_1k_5 + k_1k_3} \quad (4)$$

$$K_i = \frac{k_2k_4 + k_1k_5 + k_1k_3}{k_1k_4} \quad (5)$$

In this model, K_i and K_m are both complex kinetic constants that contain contributions from the chemical steps (k_3 and k_4) and do not correspond to dissociation constants. This situation contrasts with the model in which inhibition is due to binding at a third, inhibitory site on the enzyme. The third-site model predicts that K_i and K_d for the inhibitory metal ion are identical. Equation 2 can be derived for a partially ordered mechanism in which a relatively minor pathway for release of product without prior release of metal ion is present. Such a model leads to K_{in} being a kinetic constant that is not equivalent to the dissociation constant for the metal ion.

Scheme 2

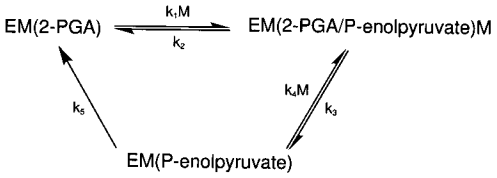

Kinetic Isotope Effects. Primary deuterium kinetic isotope effects on the rate of dehydration of 2-PGA were determined by direct comparison of initial rates measured with saturating [2-^{1}H]-2-PGA or [2-^{2}H]-2-PGA and varied metal ion concentrations. Data were fitted to eq 2 for Mg^{2+} and Mn^{2+} and to eq 1 for Zn^{2+}. The assumption that the isotope effect approaches unity at infinite [M^{2+}] leads to a relationship between $^DK_{in}$, $^DK_{id}$, and ^DV (eq 6). Use of eq 6 to calculate $^DK_{id}$ in the fitted model lowered the uncertainty of the fitted parameters but did not otherwise alter the fit.

$$^DK_{id} = {}^DK_{in}\,{}^DV \quad (6)$$

EPR Measurements. Q-band (35 GHz) EPR spectra were recorded with a Varian E109Q spectrometer. The sample temperature was maintained at 273 ± 1 K with a Varian flow Dewar and temperature controller. Low-temperature spectra were recorded at X-band (~9.2 GHz) with a Varian E Line spectrometer equipped with an E-102 microwave bridge and an Oxford Instruments ESR 900 continuous-flow helium cryostat. Both spectrometers were interfaced with AT microcomputers for data acquisition.

Analysis of Mn^{2+}−Mn^{2+} Spin Exchange Coupling. For an isolated Mn^{2+} ($S = {}^5/_2$), bound in a complex with a protein, the dominant EPR signals arise from the $m_s = {}^1/_2$, $m_s = -{}^1/_2$ electron spin transition. Hyperfine coupling to the nuclear spin of ^{55}Mn ($I = {}^5/_2$) splits this transition into a sextet. In complexes with octahedral geometry, the ^{55}Mn hyperfine splitting constant, $|A|$, is ~90 G. Whenever two manganous ions are exchange coupled, the spectrum becomes more complicated (*38*). The two $S = {}^5/_2$ centers couple into a manifold of new spin states, with total spin $\mathbf{S} = 0, 1, 2, 3, 4, 5$. Each of the $\mathbf{S} > 0$ states contains a manifold of energy levels. Transitions between the levels within each **S** state can give rise to EPR signals. The sign and magnitude of the exchange coupling constant **J** determine the relative energies of the **S** states (*39*). Spin coupling is easily recognized in an EPR spectrum because of the appearance of 11 line patterns with relative intensities 1:2:3:4:5:6:5:4:3:2:1 in which the ^{55}Mn hyperfine spacing is ~45 G (*40*).

Determination of the Mn^{2+}−Mn^{2+} Exchange Coupling Constant. The magnitude of the Mn^{2+}−Mn^{2+} exchange coupling constant, **J**, for enolase complexed with two Mn^{2+} ions and a mixture of 2-PGA and P-enolpyruvate was determined by analysis of the intensity of the EPR signal from the $\mathbf{S} = 1$ (triplet) state as a function of temperature. The temperature dependence of the population of the spin states is governed by Boltzmann's law. Equation 7 gives the

temperature dependence of the population of the $\mathbf{S} = 1$ state of an antiferromagnetically coupled $Mn^{2+}-Mn^{2+}$ pair:

$$\text{peak height} = \frac{3e^{(-J/kT)}}{1 + 3e^{(-J/kT)} + 5e^{(-3J/kT)} + 7e^{(-6J/kT)} + 9e^{(-10J/kT)} + 11e^{(-15J/kT)}} \quad (7)$$

where J is $|\mathbf{J}|$, and k is Boltzmann's constant.

Preparation of Samples Containing ^{17}O. The concentrations of stock solutions of ^{16}O and ^{17}O compounds were matched to within ±5%. Duplicate samples containing ^{16}O or ^{17}O compounds were prepared for experiments measuring ^{17}O-induced, inhomogeneous broadening of the EPR signal. The amplitudes of EPR signals from these duplicates agreed within ±3%.

Analysis of EPR of ^{17}O-Containing Complexes. The first derivative EPR spectrum of protein-bound Mn^{2+} is usually dominated by signals from the $m_s = {}^1/_2$, $m_s = -{}^1/_2$ fine structure transition. Second-order effects of ligand-induced zero-field splitting contribute additional structure to the spectrum. Since the structure due to zero-field splitting is a product of the ligand environment of the metal, it can assist in identifying complexes. Whenever one of the ligand atoms of Mn^{2+} is ^{17}O, the EPR signals are split by superhyperfine coupling to the ^{17}O nucleus ($I = {}^5/_2$). The magnitude of the coupling is usually smaller than the line width of the signal. Therefore, the superhyperfine splitting is unresolved, but it does result in inhomogeneous broadening of the spectrum (*41*). Oxygen ligands were assigned on the basis of observation of this inhomogeneous broadening. The number of oxygen ligands contributed by P-enolpyruvate was determined by quantitative analysis of the ^{17}O-induced inhomogeneous broadening using the spectral subtraction method (*41*−*44*). A series of difference spectra are constructed by subtracting various fractions F_n (eq 8) of the spectrum of the unlabeled sample from the spectrum of the labeled sample.

$$F_n = (1 - F_{^{17}O})^n \quad (8)$$

In eq 8 $F_{^{17}O}$ is the fractional enrichment of ^{17}O. Each difference spectrum corresponds to a different number, n, of oxygen ligands contributed to Mn^{2+} by the labeled molecule. Whenever the trial value of n is smaller than the actual number of oxygen ligands contributed by the labeled molecule, a negative image of the spectrum of the unlabeled sample appears in the difference spectrum. The smallest value of n that does not produce this negative image is the smallest number of ^{17}O ligand atoms contributed by the labeled molecule which is consistent with the data.

RESULTS AND DISCUSSION

Structural Studies by Mn^{2+} EPR. The first crystals of enolase suitable for X-ray diffraction were grown using $(NH_4)_2SO_4$ as the precipitant (*45*), and several structures of yeast enolase (*46*−*51*) and one of lobster enolase (*11*) have been obtained from crystals grown under such conditions. These structures have contained at most one metal ion bound in the active site. On the basis of these structures together with data from site-directed mutagenesis and NMR relaxation studies, arguments have been made for a wide (6−12 Å) separation between the required metal ions (*26*), alternative coordination geometry between the substrate and the metal ions (*15*), and different acid/base catalysts (*11*−*13*).

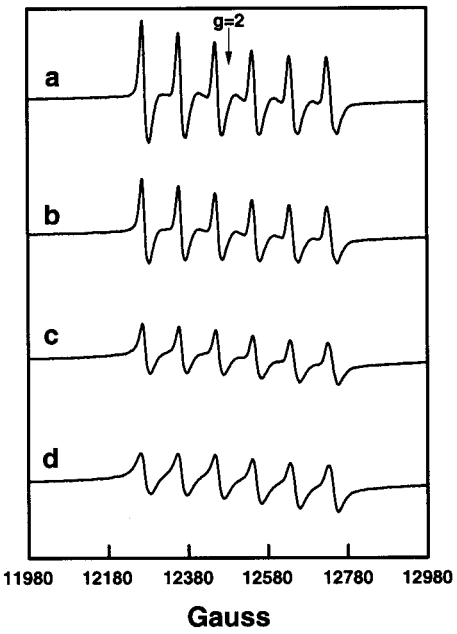

FIGURE 2: Q-band (35 GHz) spectra at 273 K of complexes of enolase, 3-hydroxy-2-nitro-1-phosphonopropane, and Mn^{2+}, illustrating the decrease in signal amplitude with increasing Mn^{2+} concentration observed for complexes with this inhibitor. The stock solution of inhibitor used was adjusted to pH 10 with 10 N KOH prior to use to convert the inhibitor to its nitronate anion, and all samples contained 0.02 M TAPS/KOH, pH 8.5. Spectra: (a) 0.98 Mn^{2+} per enolase active site, 4.2 mM enolase active sites, 4.1 mM $MnCl_2$, 6.8 mM inhibitor; (b) 1.4 Mn^{2+} per enolase active site, 3.7 mM enolase active sites, 5.0 mM $MnCl_2$, 5.9 mM inhibitor; (c) 1.7 Mn^{2+} per enolase active site, 3.3 mM enolase active sites, 5.5 mM $MnCl_2$, 5.3 mM inhibitor; (d) 2.0 Mn^{2+} per enolase active site, 3.0 mM enolase active sites, 5.9 mM $MnCl_2$, 4.9 mM inhibitor.

The amplitudes of EPR signals arising from a protein complex of Mn^{2+} are normally proportional to the total concentration of Mn^{2+}. Hence, when Mn^{2+} is added to a sample containing an excess of enzyme, the signals from the $E-Mn^{2+}$ complex typically increase approximately linearly with added Mn^{2+}. An exception can occur whenever there are two binding sites for metal ions that are closely spaced such that the electron spin−spin interactions between the two Mn^{2+} ions become significant. For example, whenever Mn^{2+} is added to a sample of pyruvate kinase, oxalate, and ATP, the signal reaches a maximum near 1 Mn^{2+} per active site and declines at higher $[Mn^{2+}]$ (*42*). The two metal ions in the complex of pyruvate kinase have been shown by EPR (*42*) and by X-ray crystallography (*20*) to be bridged by the γ-phosphate of ATP. Similar behavior is observed with enolase whenever Mn^{2+} is added to a sample of enolase containing saturating concentrations of P-enolpyruvate/2-PGA or the inhibitor 3-hydroxy-2-nitro-1-phosphonopropane[2] (*27*) (Figure 2).

Further evidence of the coupling between the two Mn^{2+} ions at the active site of enolase is found in the EPR spectrum recorded at 4 K. At this temperature the spectrum (Figure

[2] Use of the inhibitor, 3-hydroxy-2-nitro-1-phosphonopropane, in the titration eliminates complications from free Mn^{2+} because the affinity of the inhibitor complex for the second equivalent of Mn^{2+} is higher than that of the substrate/product complex.

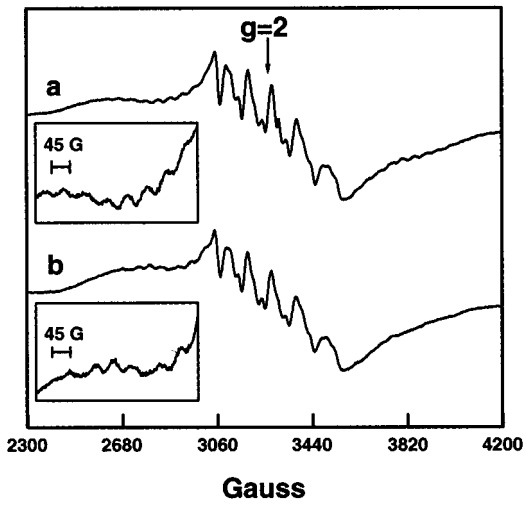

FIGURE 3: X-band (9 GHz) spectra at 4 K of complexes of enolase and Mn^{2+} exhibiting resolved 45 G hyperfine lines. (a) Complex of enolase, Mn^{2+}, and the inhibitor 3-hydroxy-2-nitro-1-phosphonopropane; 0.28 mM enolase active sites, 0.54 mM $MnCl_2$, 0.46 mM inhibitor, 0.05 M TAPS/KOH, pH 8.5. Inset: Expansion of the spectrum from 2600 to 3000 G. (b) Complex of enolase, Mn^{2+}, and P-enolpyruvate−2-PGA equilibrium mixture; 0.24 mM enolase active sites, 0.45 mM $MnCl_2$, 15 mM P-enolpyruvate, 0.04 M TAPS/KOH, pH 8.5. Inset: Expansion of the spectrum from 2600 to 3000 G.

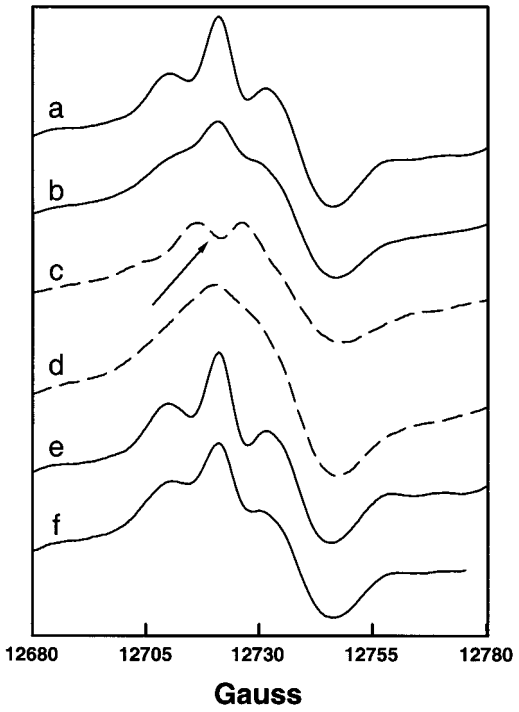

FIGURE 4: Sixth hyperfine line of spectra of complexes of enolase, Mn^{2+}, Zn^{2+}, and P-enolpyruvate. (a) Unlabeled P-enolpyruvate. (b) Uniformly ^{17}O-labeled P-enolpyruvate. Samples a and b contained 6.7 mM enolase active sites, 1.8 mM $MnCl_2$, 6.7 mM $Zn(OAc)_2$, 12 mM P-enolpyruvate, 90 mM KCl, and 0.04 M Hepes/KOH, pH 7.5. (c) Difference spectrum obtained assuming one oxygen ligand from the labeled positions of the substrate as a ligand of Mn^{2+} (spectrum b minus 51% of spectrum a). The arrow indicates the location of the negative image of the ^{16}O spectrum. (d) Difference spectrum obtained assuming two oxygens from the labeled positions of the substrate as ligands of Mn^{2+} (spectrum b minus 27% of spectrum a). (e) Unlabeled P-enolpyruvate. (f) P-enolpyruvate labeled with ^{17}O in the carboxylate oxygens. Samples e and f contained 6.4 mM enolase active sites, 1.9 mM $MnCl_2$, 6.5 mM $Zn(OAc)_2$, 11 mM P-enolpyruvate, 79 mM KOAc, and 0.04 M Hepes/KOH, pH 7.5.

3) contains signals displaying ^{55}Mn hyperfine lines spaced ~45 G apart, characteristic of spin exchange coupled Mn^{2+}−Mn^{2+} pairs. Analysis of the temperature dependence of the spin exchange coupled signals from the complex of enolase with substrate and two Mn^{2+} reveals that the signals exhibiting the 45 G hyperfine splitting arise from the triplet ($\mathbf{S} = 1$) state of the spin-coupled pair and that the coupling is antiferromagnetic ($\boldsymbol{J} = 2.7 \pm 0.2$ cm^{-1}). Antiferromagnetic coupling suggests that the exchange is mediated by a bridging ligand, consistent with the crystallographic observation that one of the carboxylate oxygens bridges the metal ions (*9*). The population of the triplet state becomes too small to generate detectable EPR signals above 40 K. Hence, observation of exchange-coupled signals near 4 K does not contradict earlier reports of the apparent absence of such signals from a similar sample at 77 K (*52*).

Coordination of Mn^{2+} to oxygen atoms of substrates or inhibitors in enzymic complexes can be determined through the use of EPR and ^{17}O labeling (*53*). To apply this technique to complexes of enolase, one must first eliminate Mn^{2+}−Mn^{2+} spin coupling. Spin coupling can be eliminated by replacing one of the manganous ions with a diamagnetic ion (*42*, *54*, *55*). When 1 equiv of Zn^{2+} is added to a sample of enolase containing a saturating amount of P-enolpyruvate/2-PGA and 0.1−0.2 equiv of Mn^{2+}, a sharp distinctive Mn^{2+} EPR spectrum is obtained. The height of this signal is linear in Mn^{2+} concentration up to 1 equiv of Mn^{2+} (2 equiv of metal ion), indicating a lack of Mn^{2+}−Mn^{2+} spin coupling (*4*). This change in the concentration dependence of the Mn^{2+} EPR spectrum in the presence of Zn^{2+} together with the change in the shape of the spectrum when Zn^{2+} is added shows that ~1 equiv of Zn^{2+} binds to the enzyme under these conditions. Substitution of uniformly ^{17}O-labeled P-enolpyruvate for P-enolpyruvate broadens the spectrum of the complex of enolase, Zn^{2+}, Mn^{2+}, and P-enolpyruvate/2-PGA (Figure 4a,b). Spectral subtraction analysis (Figure 4c,d) reveals that P-enolpyruvate contributes two oxygen ligands to Mn^{2+} in this complex. When P-enolpyruvate labeled with ^{17}O only in the carboxylate is used, broadening corresponding to one ^{17}O ligand is observed (Figure 4e,f). Thus Mn^{2+} is coordinated to one phosphate and one carboxylate oxygen of P-enolpyruvate/2-PGA in this complex (Scheme 3). The coordination of Mn^{2+} to one phosphate and one carboxylate oxygen of the substrate in the Zn^{2+}/Mn^{2+} hybrid complex indicates that Mn^{2+} resides at the second metal ion binding site in this complex. Location of Mn^{2+} at the second site implies that Zn^{2+} preferentially occupies the first site, and this conjecture is supported by the observation that 1 equiv of Zn^{2+} is needed to produce the observed spectrum. The fact that the present data are obtained from samples having a total divalent metal ion content of 1.2 equiv per active site makes it unlikely that metal ions are binding to a third, lower affinity, "inhibitory" site in this complex. The coordination

Scheme 3

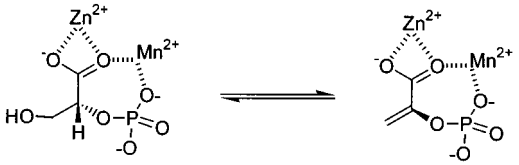

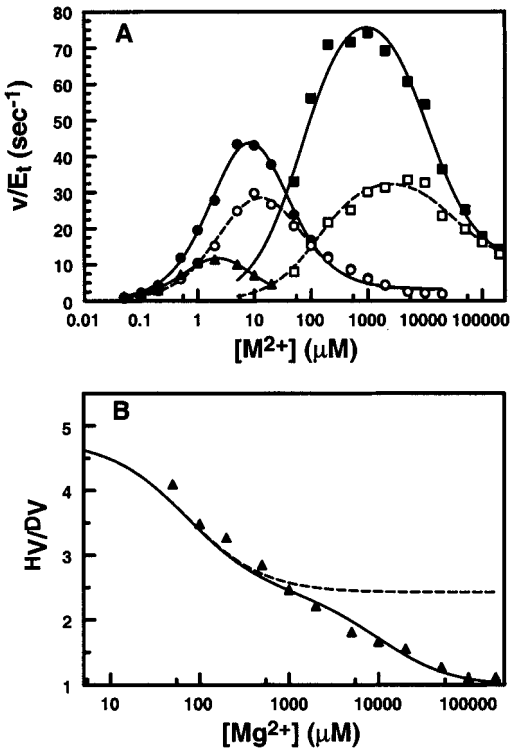

FIGURE 5: (A) Metal ion activation/inhibition of and primary deuterium kinetic isotope effect on the enolase-catalyzed dehydration of 2-PGA. Samples contained 0.05 M Hepes adjusted to pH 7.5 with KOH, $MgCl_2$ (□, ■), $MnCl_2$ (○, ●), or $CoCl_2$ (▲) as indicated and either 1 mM 2-PGA (closed symbols and solid lines) or 1 mM [2-^{2}H]-2-PGA (open symbols and dashed lines). Smooth curves represent fits to eq 2. (B) Dependence of the deuterium kinetic isotope effect on [Mg^{2+}]. Solid line: isotope effect predicted by the predominantly ordered mechanism (eq 2 with parameters from Tables 1 and 2). Dashed line: isotope effect predicted for the mechanism with inhibition by ancillary metal ion binding (eq 2 with no isotope effect on K_{in} or K_{id}). Data are as in panel A.

of Mn^{2+} at the second site and Zn^{2+} at the first site deduced from EPR measurements with ^{17}O-labeled substrate/product is completely consistent with the coordination of the Mg^{2+} ions and with the role of the carboxylate oxygen as a bridging ligand between the two metal ions observed crystallographically (*9*). Agreement between the metal ion coordination scheme deduced from EPR measurements made on samples of active enzyme in solution and that obtained from the structure derived from crystals grown at pH 8 in PEG at low ionic strength reinforces the notion that these structures are relevant to the activation of enolase by metal ions.

Kinetics of Metal Ion Activation and Inhibition. An ordered mechanism for binding of substrate and the second metal ion to enolase (Scheme 1 and eq 1) provides a simpler explanation for the observed inhibition at higher concentrations of metal ion than the hypothesis of a third, ill-defined, binding site. However, the metal activation profiles of neither the forward (Figure 5) nor the reverse reaction of enolase fit exactly to the model of a strictly ordered mechanism. Rather, the activation curves of both reactions fit better to eq 2, which includes the possibility of a second, minor, pathway of release of product without prior release of the second metal ion. In the minor pathway release of product is independent of concentration of metal ion. The relative rates of these pathways can be estimated from the metal ion activation curve. The usual ordered pathway is inoperative at infinite concentration of metal ion so that the extrapolated rate at infinite concentration of metal ion represents the rate of the second pathway. The ratio of this rate to V_{max} is a measure of the importance of the alternate pathway or randomness. In terms of eq 2 this ratio is K_{in}/K_{id}. Kinetic parameters for activation by different species of metal ion are summarized in Table 1.

The predominantly ordered mechanism not only explains the inhibition of enolase at higher concentrations of metal ion but also predicts that when the concentration of metal ion is higher than optimal, release of products from the enzyme should become substantially rate limiting. Primary deuterium kinetic isotope effects measured with [2-^{2}H]-2-PGA approach unity at inhibitory concentrations of metal ion—an observation that is consistent with this prediction (Figure 5, Table 2)[3] (*1*). The convergence of the rates of dehydration of protio and deuterio 2-PGA at inhibitory concentrations of metal ion is due to a shift of the inhibitory limb of the activation curve to higher concentrations for the deuterio substrate. This shift appears as an inverse isotope effect on the K_i's. The isotope effect on K_i is required if inhibition is the result of an ordered mechanism, but it is impossible if inhibition is due to binding at a third site which is insensitive to chemistry. Hence, the observed isotope effects are *inconsistent* with the predictions based on a model for which inhibition is due to binding of metal ions to a third site on the enzyme (*12*, *22*). The "third site hypothesis" implies that the flux at inhibitory concentrations of metal ion is carried by a subpopulation of the enzyme which bears only 2 equiv of metal ion. This subpopulation would be expected to give the same isotope effect at all concentrations of metal ion (Figure 5B, dashed line).

Co^{2+} and Zn^{2+} are more electrophilic than Mg^{2+} and might, therefore, be expected to be more efficient at promoting the ionization of the C2 proton. Co^{2+} and Zn^{2+} both, however, give lower maximal activity with enolase than does Mg^{2+} (Figure 5, Table 1). If steps other than ionization of the C2 proton are substantially rate limiting, the ^{2}H kinetic isotope effect for deuterium at C2 should be small. The measured isotope effect for Co^{2+} was unity at saturating [Co^{2+}] and only slightly above noise (~10%) at subsaturating [Co^{2+}] (data not shown). The ^{2}H isotope effects for activation by Zn^{2+} in noncomplexing buffers are also small (Figure 6). These results indicate that abstraction of the C2 proton is not rate limiting for Zn^{2+} and Co^{2+} under these conditions.

In early studies (*21*) on metal ion activation of enolase, imidazole was used as a buffer and as a complexing agent to improve the solubility of the transition metal ions. With Zn^{2+} as the activating metal ion, addition of imidazole to the assay results in a substantial increase in the maximum rate. The size of this increase varies with the concentration of imidazole added and reaches a maximum around 30 mM imidazole (Figure 6a). Addition of imidazole also causes a large increase in the amount of Zn^{2+} required to achieve the maximum rate. Interestingly, [$Zn(H_2O)_6^{2+}$] at the optimum [$ZnCl_2$] in the presence of 30 mM imidazole is much less than the [$ZnCl_2$] required to achieve the maximum rate in the absence of imidazole. At 30 mM imidazole and 200 μM

[3] The ^{2}H kinetic isotope effects reported here for enolase activation by Mg^{2+}, Mn^{2+}, and Co^{2+} generally agree with values reported previously by Shen and Westhead (*1*).

Table 1: Kinetic Parameters for Metal Ion Activation/Inhibition of Enolase

metal ion (substrate)	k_{cat} (s^{-1})	k_{cat}/K_m ($s^{-1}\,\mu M^{-1}$)	K_{in} (mM)	K_{id} (mM)	fraction of randomness
Mg^{2+} (2-PGA)	84 ± 3	1.4 ± 0.1	12 ± 2	100 ± 40	0.1
Mg^{2+} (P-enolpyruvate)	15.6 ± 0.6	1.3 ± 0.2	15 ± 5	70 ± 40	0.2
Mn^{2+} (2-PGA)	72 ± 4	26 ± 2	0.024 ± 0.003	0.54 ± 0.09	0.04
Zn^{2+} (2-PGA)	32 ± 4	11 ± 1	0.012 ± 0.003	0.3 ± 0.1	0.04
Co^{2+} (2-PGA)	31 ± 5	17 ± 2	≤0.009	0.15 ± 0.02	~0.02

Table 2: Primary Deuterium Kinetic Isotope Effects on the Enolase-Catalyzed Dehydration of 2-PGA[a]

metal ion	$^{D}(V/K)_M$	^{D}V	$^{D}K_{i(n)}$	$^{D}K_{id}$
Mg^{2+}	6 ± 1	2.3 ± 0.2	0.4 ± 0.1	0.9 ± 0.1
Mn^{2+}	1.9 ± 0.2	1.7 ± 0.2	0.5 ± 0.1	0.8 ± 0.1
Zn^{2+}	1.6 ± 0.1	0.98 ± 0.04	1	
Zn^{2+} (30 mM imidazole)	3.2 ± 0.4	1.5 ± 0.2	0.3 ± 0.2	

[a] Parameters for Mg^{2+} and Mn^{2+} were obtained by fitting data to eq 2; parameters for Zn^{2+} were obtained by fitting data to eq 1.

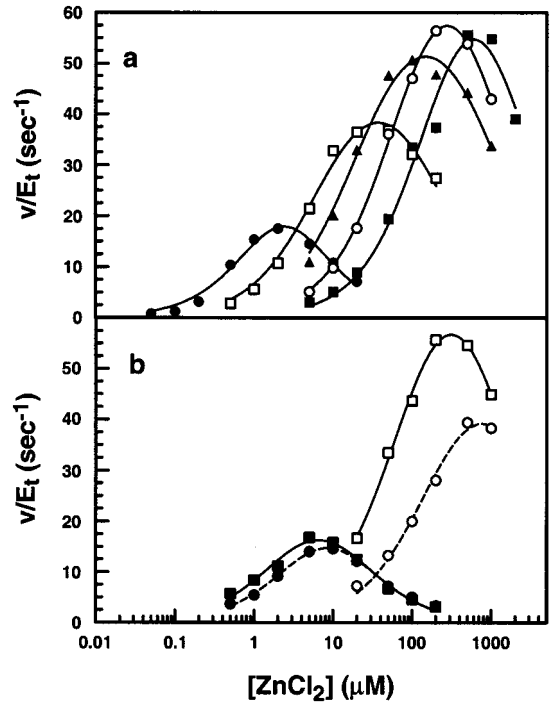

FIGURE 6: (a) Effect of imidazole on Zn^{2+}-activated enolase. Samples contained 0.05 M Hepes adjusted to pH 7.5, 1 mM 2-PGA, and 0 (●), 10 (□), 20 (▲), 30 (○), or 40 (■) mM imidazole. Smooth curves represent fits to eq 1. (b) Primary deuterium isotope effect on the Zn^{2+}-activated enolase-catalyzed dehydration of 2-PGA in the presence and absence of imidazole. Samples contained 0.05 M Hepes adjusted to pH 7.5, 0.03 M imidazole (open symbols) or no imidazole (closed symbols), and 1 mM 2-PGA (squares and solid lines) or 1 mM [2-^{2}H]-2-PGA (circles and dashed lines). Smooth curves represent fits to eq 2 for the data in the absence of imidazole or to eq 1 for the data in 0.03 M imidazole.

$ZnCl_2$, the approximate distribution of Zn^{2+} among the various complexes is predicted to be the following: Zn(imidazole)$_4(H_2O)_2^{2+}$, 0.13 mM; Zn(imidazole)$_3(H_2O)_3^{2+}$, 50 μM; Zn(imidazole)$_2(H_2O)_4^{2+}$, 14 μM; Zn(imidazole)$(H_2O)_5^{2+}$, 3 μM; and $Zn(H_2O)_6^{2+}$, 0.4 μM. The concentration of Zn$(H_2O)_6^{2+}$ is clearly too low to produce the level of activity that is observed under these conditions. However, the concentrations of Zn(imidazole)$_{1-3}^{2+}$ are in the range expected to produce high activity. Hence, it appears that the enzyme is able to extract Zn^{2+}, needed for population of its binding sites, from Zn^{2+} species in which water ligands have been replaced by one or more imidazole ligands. The ^{2}H isotope effect observed with Zn^{2+}-activated enolase is substantially increased by addition of 30 mM imidazole (Figure 6b, Table 2). The increase in rate and ^{2}H isotope effect support the notion that imidazole accelerates the release of Zn^{2+} from the product complex.

The catalytic acid and base of enolase are left in the wrong protonation state for dehydration following release of P-enolpyruvate. One might argue that imidazole could accelerate the reaction by catalyzing the isomerization to the correct protonation state. This scenario seems unlikely, however, because there is little effect of imidazole when Mg^{2+}, a metal ion for which imidazole has little affinity, is used. Another explanation is that imidazole is masking the effect of some contaminating inhibitory metal ion. If this were the case, the effect of imidazole might vary when different batches of $ZnCl_2$ of varying purity are used. No such variation in the reaction rate or the effect of imidazole was observed when different sources of $ZnCl_2$ were compared.

Conclusions. The Mn^{2+} EPR evidence presented confirms the coordination scheme for the second metal ion in enolase and thus supports the idea that both of the metal ions required by enolase coordinate to the carboxylate group of the substrate/product. In this structure, the metal ions are positioned to promote ionization of 2-PGA and to stabilize the enolate intermediate. The disappearance of the primary deuterium isotope effect on the dehydration of 2-PGA at inhibitory concentrations of metal ion shows that the observed bell-shaped metal ion activation curves are the result of a predominantly ordered mechanism and not due to binding at a separate "inhibitory" site. The case for an ordered mechanism is reinforced, and the contribution of metal ion release to the overall rate is demonstrated by the imidazole enhancement of enolase activity with Zn^{2+}.

ACKNOWLEDGMENT

The authors thank Drs. Sandra, Matthew, and Robert Johnson for assistance in modeling the mass spectrum of ^{17}O-labeled PEP and Dr. Todd Larsen for assistance with molecular graphics.

REFERENCES

1. Shen, T. Y. S., and Westhead, E. W. (1973) *Biochemistry 12*, 3333−3337.
2. Dinovo, E. C., and Boyer, P. D. (1971) *J. Biol. Chem. 246*, 4586−4593.
3. Anderson, S. R., Anderson, V. E., and Knowles, J. R. (1994) *Biochemistry 33*, 10545−10555.
4. Poyner, R. R., Laughlin, L. T., Sowa, G. A., and Reed, G. H. (1996) *Biochemistry 35*, 1692−1699.
5. Lebioda, L., and Stec, B. (1991) *Biochemistry 30*, 2817−2822.

6. Brewer, J. M., Robson, R. L., Glover, C. V., Holland, M. J., and Lebioda, L. (1993) *Proteins: Struct., Funct., Genet. 17*, 426−434.
7. Sangadala, V. S., Glover, C. V., Robson, R. L., Holland, M. J., Lebioda, L., and Brewer, J. M. (1995) *Biochim. Biophys. Acta 1251*, 23−31.
8. Wedekind, J. E., Poyner, R. R., Reed, G. H., and Rayment, I. (1994) *Biochemistry 33*, 9333−9342.
9. Larsen, T. M., Wedekind, J. E., Rayment, I., and Reed, G. H. (1996) *Biochemistry 35*, 4349−4358.
10. Reed, G. H., Poyner, R. R., Larsen, T. M., Wedekind, J. E., and Rayment, I. (1996) *Curr. Opin. Struct. Biol. 6*, 736−743.
11. Duquerroy, S., Camus, C., and Janin, J. (1995) *Biochemistry 34*, 12513−12523.
12. Vinarov, D. A., and Nowak, T. (1998) *Biochemistry 37*, 15238−15246.
13. Vinarov, D. A., and Nowak, T. (1999) *Biochemistry 38*, 12138−12149.
14. Lis, T. (1985) *Acta Crystallogr., Sect. C: Cryst. Struct. Commun. 41*, 1578−1580.
15. Nowak, T., Mildvan, A. S., and Kenyon, G. L. (1973) *Biochemistry 12*, 1690−1701.
16. Zhang, E., Brewer, J. M., Minor, W., Carreira, L. A., and Lebioda, L. (1997) *Biochemistry 36*, 12526−12534.
17. Brewer, J. M., Glover, C. V., Holland, M. J., and Lebioda, L. (1997) *Biochim. Biophys. Acta 1340*, 88−96.
18. Cohn, M., Pearson, J. E., O'Connell, E. L., and Rose, I. (1970) *J. Am. Chem. Soc. 92*, 4095−4098.
19. Faller, L. D., Baroudy, B. M., Johnson, A. M., and Ewall, R. X. (1977) *Biochemistry 16*, 3864−3869.
20. Larsen, T. M., Benning, M. M., Rayment, I., and Reed, G. H. (1998) *Biochemistry 37*, 6247−6255.
21. Wold, F., and Ballou, C. E. (1957) *J. Biol. Chem. 227*, 313−328.
22. Brewer, J. M., and Lebioda, L. (1997) *Adv. Biophys. Chem. 6*, 111−141.
23. Rose, S. L., Dickinson, L. C., and Westhead, E. W. (1984) *J. Biol. Chem. 259*, 4405−4413.
24. Cleland, W. W. (1970) in *The Enzymes* (Boyer, P. D., Ed.) pp 1−65, Academic Press, New York.
25. Anderson, V. E. (1981), Ph.D. Dissertation, University of Wisconsin.
26. Lee, M. E., and Nowak, T. (1992) *Arch. Biochem. Biophys. 293*, 264−273.
27. Anderson, V. E., Weiss, P. M., and Cleland, W. W. (1984) *Biochemistry 23*, 2779−2786.
28. McKenna, C. E., Higa, M. T., and Cheung, N. H. (1977) *Tetrahedron Lett. 18*, 155.
29. O'Neal, C. C., Jr., Bild, G. S., and Smith, L. T. (1983) *Biochemistry 22*, 611−617.
30. Lodato, D. T. (1986), Ph.D. Dissertation, University of Pennsylvania.
31. Warburg, O., and Christian, W. (1941) *Biochem. Z. 310*, 384−421.
32. Chin, C. C. Q., Brewer, J. M., Eckard, E., and Wold, F. (1981) *J. Biol. Chem. 256*, 1377−1384.
33. Holland, M. J., Holland, J. P., Thill, G. P., and Jackson, K. A. (1981) *J. Biol. Chem. 256*, 1285−1395.
34. Sillen, L. G., and Martell, A. E. (1964) *Stability Constants of Metal Ion Complexes*, The Chemical Society, London.
35. Wold, F., and Ballou, C. E. (1957) *J. Biol. Chem. 227*, 301−312.
36. Kyte, J. (1995) *Mechanism in protein chemistry*, Garland Publishing, Inc., New York.
37. Cleland, W. W. (1975) *Biochemistry 14*, 3220−3224.
38. Abragam, A., and Bleany, B. (1970) *Electron paramagnetic resonance of transition ions*, Oxford University Press, London.
39. Owen, J., and Harris, E. A. (1972) in *Electron Paramagnetic Resonance* (Geschwind, S., Ed.) pp 427−492, Plenum, New York.
40. Weltner, W. (1983) in *Magnetic Atoms and Molecules*, pp 235−322, Dover, New York.
41. Reed, G. H., and Leyh, T. S. (1980) *Biochemistry 19*, 5472−5480.
42. Lodato, D. T., and Reed, G. H. (1987) *Biochemistry 26*, 2243−2250.
43. Smithers, G. W., Poe, M., Latwessen, D. G., and Reed, G. H. (1990) *Arch. Biochem. Biophys. 280*, 416−420.
44. Reed, G. H., and Poyner, R. R. (2000) *Met. Ions Biol. Syst. 37*, 183−207.
45. Lebioda, L., and Brewer, J. M. (1984) *J. Mol. Biol. 180*, 213-215.
46. Lebioda, L., and Stec, B. (1989) *J. Am. Chem. Soc. 111*, 8511−8513.
47. Lebioda, L., Stec, B., and Brewer, J. M. (1989) *J. Biol. Chem. 264*, 3685−3693.
48. Lebioda, L., and Stec, B. (1991) *Biochemistry 30*, 2817−2822.
49. Lebioda, L., Stec, B., Brewer, J. M., and Tykarska, E. (1991) *Biochemistry 30*, 2823−2827.
50. Lebioda, L., Zhang, E., Lewinski, K., and Brewer, J. M. (1993) *Proteins: Struct., Funct., Genet. 16*, 219−225.
51. Stec, B., and Lebioda, L. (1990) *J. Mol. Biol. 211*, 235−248.
52. Chien, J. C. W., and Westhead, E. W. (1971) *Biochemistry 10*, 3198−3203.
53. Reed, G. H., and Markham, G. D. (1984) *Biol. Magn. Reson. 6*, 73−142.
54. Buchbinder, J. L., and Reed, G. H. (1990) *Biochemistry 29*, 1799−1806.
55. Poyner, R. R., and Reed, G. H. (1992) *Biochemistry 31*, 7166−7173.
56. Kraulis, P. J. (1991) *J. Appl. Crystallogr. 24*, 946−950.
57. Merritt, E. A., and Bacon, D. J. (1997) *Methods Enzymol. 277*, 505−524.
58. Brewer, J. M., Holland, M. J., and Lebioda, L. (2000) *Biochem. Biophys. Res. Commun. 276*, 1199−1202.

BI0103922